Temporally resolved PLIF measurements of the temperature inside droplets impinging on a hot solid surface

William Chaze, Romain Collignon, Ophélie Caballina, Guillaume Castanet, Fabrice Lemoine

Temporally resolved PLIF measurements of the temperature inside droplets impinging on a hot solid surface

William Chaze, Romain Collignon, Ophélie Caballina, Guillaume Castanet*, Fabrice Lemoine
Université de Lorraine, CNRS, LEMTA, F-54000 Nancy, France
* Correspondent author: guillaume.castanet@univ-lorraine.fr

Keywords: Laser-Induced fluorescence, Temperature field measurement, Drop impact, Film boiling

ABSTRACT

Heat transfers at the impact of a droplet on a hot solid surface are investigated experimentally. Millimeter-sized droplets impinge a heated flat sapphire window. The time evolution of the droplet temperature is characterized using the two-color laser-induced fluorescence technique. For that, a Q-switched Nd:YAG laser is used for the excitation of the fluorescence in order to obtain instantaneous images of the droplet temperature. The fluid under investigation is seeded with two fluorescent dyes, one sensitive to temperature (fluorescein disodium) and the other not (sulforhodamine 640). Owing to a wavelength shift between the dyes' emissions, the fluorescence signal of the dyes can be detected separately by two cameras. The liquid temperature is determined with a good accuracy by doing the ratio of the images of the dyes' fluorescence. A critical feature of the method is that the image ratio is not disturbed by the deformation of the impacting droplet, which affects the signals of the dyes almost identically. Experiments are performed in the conditions of film boiling. A thin vapor film at the interface between the droplet and the solid surface prevents the deposition of liquid on the hot solid surface. Results highlight how the temperature distribution inside a droplet evolves when it impinges on a heated solid surface in the film boiling regime. By changing the impact velocity for water and ethanol droplets, comparisons between several experimental cases show the effect of the Weber number and of the fluid properties on the heat transfers within the droplet during its interaction with the heated surface.

1. Introduction

Liquid cooling is widely used in applications, which require a high heat dissipation rate. Cooling techniques such as pool boiling or jet impingement can provide high heat dissipation rates, but they generally fail to insure a uniform cooling. Comparatively, spray cooling technology is of increasing interest since it is characterized by high heat transfer rates, uniformity of heat removal and small fluid inventory. In electronic systems and power electronics, spray cooling is required to maintain lower operating temperature of the component. In the steel industry, environmental and economic constraints have imposed greater demands for a reduction of the water and energy consumptions. Spray quenching is very efficient compared to other cooling techniques. The main reason is that vapor can easily escape even if the temperature of the wall is well above

the Leidenfrost temperature. However, while this cooling technology is applied for decades, its integration remains a complex and cumbersome process because of still incomplete knowledge of the fluid flow and heat transfer characteristics. In particular, scientific investigations focused on individual droplets are still required to understand the underlying physics behind the interactions between droplets and a hot solid surface.

The investigation of the impingement of droplets on solid surfaces has received a considerable attention throughout the decades. When a drop impacts a hot wall, different behaviors can occur: the drop can spread over the solid surface and remain attached to it due to wettability forces. It can splash and create several smaller secondary droplets or simply rebound. Extensive experimental investigations were carried out to determine the parameters influencing the behavior of a single drop impact. Some of these parameters describe the geometry and the dynamic of the drops, some refer to the physical properties of the liquid or the solid surface [1]. Descriptions of an impact are usually made on the basis of correlations with dimensionless numbers characterizing the relative magnitude of the forces acting on the impinging droplet, i.e. Reynolds, Weber and Ohnesorge numbers. Regarding heat transfers, almost all the studies were focused around the heat removal from the solid surface, whose temperature was monitored using, for example, IR thermography [2, 3]. Coupled with an inverse model, these measurements made quantification of the heat removed from the wall and the cooling efficiency possible [3]. Recently, Jung *et al*. [2] used IR thermography to characterize the temporal evolution of the heat flux at the wall during the impact of millimeter-size water droplets. The contributions of liquid evaporation and liquid heating to the overall heat exchange between the droplet and the wall are not obvious to evaluate if measurements are restricted to the wall heat flux. The droplet heating can be characterized using the two-color laser-induced fluorescence thermometry (2cLIF) which is one of the few proven techniques available to measure the temperature of droplets [4]. The liquid (in this case water) is seeded by a temperature-dependent fluorescent dye. The capabilities of the technique for studying the drop impact were initially demonstrated on mono-sized droplet streams impinging obliquely a heated wall [5]. Dunand *et al*. [6] made use of a laser sheet and two cameras in order to visualize the temperature of the impacting droplets. However, using a CW laser, measurements suffer from serious limitations. Light intensity within the laser sheet was not sufficient to shorten the exposure time of the cameras enough to obtain instantaneous images of the impinging droplets. More recently, several improvements to the 2cLIF technique were made by Chaze *et al*. [7] to achieve single shot measurements of the temperature using nanosecond pulse laser.

The present study relies on these previous works for the development of optical diagnostics adapted to the characterization of heat and mass transfers at the drop impact on heated solid

surfaces. The focus is put on the film boiling regime, in which a thin vapor film at the interface between the droplet and the solid surface prevents the deposition of liquid on the wall surface. Ultimately, the experimental results will help understanding the coupling between the droplet deformation at the impact and the heat and mass transfers. For this purpose, different impact velocities for water and ethanol droplets are considered in this work.

2. Measurement technique and experimental set-up

2.1 Temperature measurements based on two-color laser-induced fluorescence

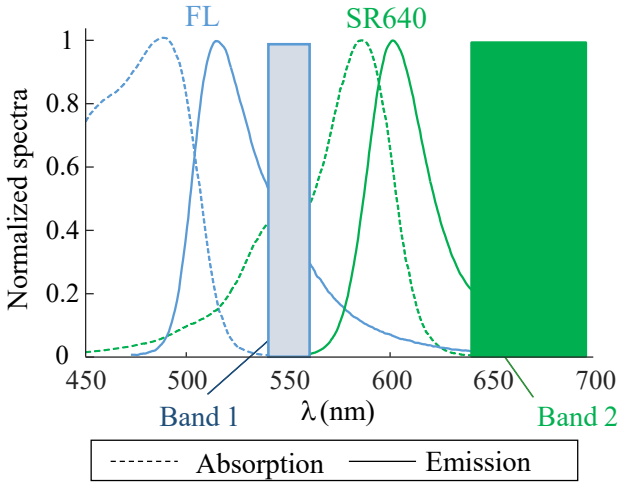

Fig. 1 The two detection bands selected for the application of the 2cLIF technique using the couple of dyes FL/SR640 in water.

The time evolution of the droplet temperature is characterized using the laser-induced fluorescence technique. The latter is one of the few proven techniques to characterize the temperature in liquids in a non-intrusive way. For some organic dyes like Rhodamine B, the fluorescence signal induced by laser excitation is known to be temperature-sensitive. For measurements to be reliable, signal variations must come exclusively from changes in temperature. However, many factors affect the intensity of the LIF signal in addition to the temperature. In particular, the signal is affected by the transmission of light into the flow. Refractive index changes, unavoidable in the presence of heat transfer, can disturb the measured signal of fluorescence. The same is true for the dispersion of light by liquid/gas interfaces in two-phase flows. The ratio R of the intensities of fluorescence signal measured by detectors operating in two different spectral bands makes it possible to eliminate most of the problems mentioned above. The methods based on a ratio of intensities are hereinafter referred to as two-

color LIF (2cLIF). In order for the fluorescence ratio R to be sensitive to temperature, a first solution consists in mixing two dyes that respond differently to the temperature [8]. Another solution is to use a dye whose emission spectrum is deformed with temperature [4]. 2cLIF techniques were mainly used to perform spot measurements using continuous lasers. Several recent works have demonstrated that it is possible to characterize temperature fields using a laser sheet to excite fluorescence. Nevertheless, a problem arises with regard to the use of pulsed lasers. Indeed, when the excitation is intense (typically a few MW/cm^2), a saturation phenomenon affects the signal of the fluorescence whose intensity F_λ at the wavelength λ is given by:

$$F_\lambda = \eta \frac{\Omega}{4\pi} \epsilon_0 \phi_\lambda \frac{I_0}{1+I_0/I_{sat}} CV \quad (1)$$

where I_0 is the intensity of the incident laser beam. The parameters ϵ_0, ϕ_λ and I_{sat} respectively denote the absorption coefficient of the dye at the wavelength of the laser, the quantum yield and the intensity of saturation of the fluorescence. C is the molar concentration of the dye molecules. η is the transmission efficiency of the fluorescence light to the detector. Ω denotes the solid angle of the collection. In Eq.(1), parameters ϵ_0, ϕ_λ and I_{sat} are temperature dependent. While ϕ_λ decreases with temperature due to collisional quenching, the saturation intensity I_{sat} follows an inverse trend [7]. As a result, fluorescent dyes can lose some of their temperature sensitivity at high laser irradiance. In the following, fluorescein disodium (FL) is used as its temperature sensitivity arises exclusively from ϵ_0 and therefore it retains a high and unchanged temperature sensitivity regardless of the laser irradiance [7]. FL is mixed with sulforhodamine 640 (SR640) whose fluorescent emission does not vary with temperature. Figure 1 shows the detection bands selected for the experiments in water. In the region [540 nm-560 nm], only FL has a contribution to the signal while the emission of SR640 is predominant above 640 nm. Taking the ratio of the signals detected in the two emission bands allows eliminating the dependence on the droplet shape, since the fluorescence emitted in the two detection bands is affected almost identically by light dispersion at the droplet surface. The ratio R of the signals in the detection bands can be determined by:

$$R = R_0 \frac{\epsilon_{0,FL}(T)}{\epsilon_{0,FL}(T_0)} \quad (2)$$

where R_0 is a reference ratio measured at a known temperature T_0.

2.2 Experimental setup

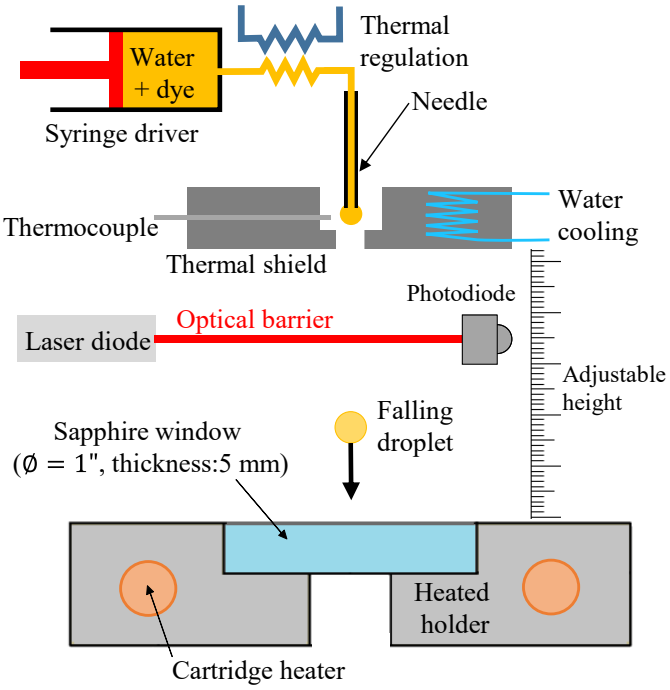

Fig. 2 The experimental setup.

The couple of dyes FL/SRh640 is used to characterize the heating of a drop during the impact with a hot solid surface in the film boiling regime. The experimental setup is presented in Figure 2. The drops are produced by means of a dropper system consisting of a syringe driver and a needle. The drops seeded with dyes are detached from the needle under the effect of their weight with a perfectly reproducible size. A 400 µm base diameter needle is used to produce water drops with a diameter of 2.5 mm and ethanol droplets with a diameter of 1.9 mm. The frequency of the droplet detachment is controlled by means of the syringe driver which allows delivering a constant liquid flow rate. The droplets fall on a sapphire window (1" in diameter and 5 mm thick), placed on a steel holder which is heated using cartridges heaters (4x250 W). Owing to the large thermal conductivity of sapphire (about 40 W/m/K), the temperature of the solid surface is uniform and nearly equal to that of the steel holder. A thermal shield is necessary to prevent heating of the liquid inside the needle caused by the hot air plume rising from the sapphire window. The tip of the needle is placed into a cavity of a few millimeters arranged inside a metallic plate which is cooled down by a water circulation. Moreover, the fluorescent solution passes into a heat exchanger before entering the needle.

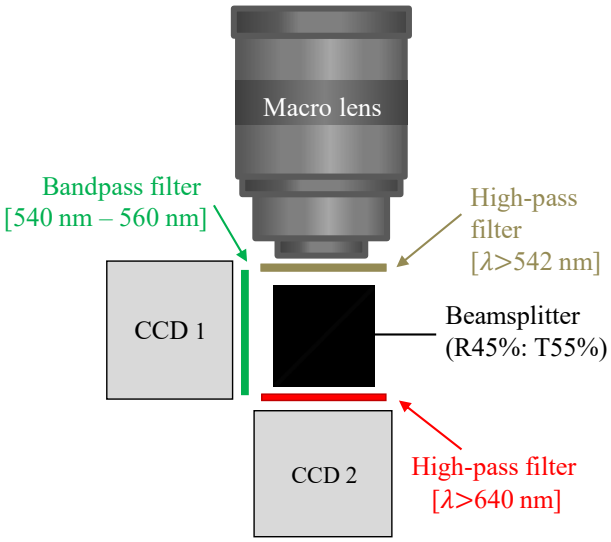

Fig. 3 Arrangement of the optical detection system.

A thermocouple, placed at a short distance from the droplet in the cavity, is used to control the ambient temperature. This provides a good approximation for the temperature of the pendant droplet, because the same setpoint is imposed in the thermal regulations with the heat exchanger and the thermal shield. The needle is moved up and down to modify the impact velocity. Finally, an aperture managed in the steel holder allows using a sapphire window for a backside illumination and/or visualization of the impinging droplet.

The laser beam coming from a pulsed Nd: YAG laser at 532 nm (Quantel Brillant B, E = 450 mJ, pulse duration dt = 5 ns) is used for the excitation of the fluorescence. The diameter of the beam (about 6 mm) is much larger than the size of the droplets, which yields an illumination of the whole liquid volume during the droplet deformation. Experiments are carried out at high laser fluence (typically I_0 >100 MW/cm^2), so that the fluorescence is saturated at each laser shot. Hence, the fluorescence emission is distributed quite uniformly inside the droplets. The repetition rate of the pulsed laser (10 Hz) is by far too low to resolve temporally a drop impact. An optical barrier consisting of a laser diode and a photodiode is placed on the trajectory of the drops at a few millimeters above the sapphire surface and makes it possible to detect the fall of a droplet. It allows the triggering of the laser pulse on the detection of a droplet by the optical barrier. The electronic device can delay the time of the laser pulse by small increments so as to explore, droplet after droplet, the whole impact period. This time reconstruction is only possible owing to the fact that droplets can be produced repeatedly with exactly the same size, velocity and trajectory when all aerodynamic perturbations are eliminated. Two CCD cameras (Allied Vision Tech Prosilica GT3300 B/C GigE Camera 3296 x 2472, 12 bit, 5.5 µm), each one equipped with an interference filter for the detection of the fluorescence in the bands presented in Fig.1,

are utilized to observe the droplets (Fig.3). The optical system also includes an objective lens (SIGMA APO MACRO 150 mm F2.8 EX DG OS HSM and its teleconverter x2) and a beamsplitter mounted in front of the cameras. Two configurations of the optical system are used to visualize the impacting droplet. A 45° tilted mirror is placed under the sapphire window and its heated holder. It makes it possible to observe the droplet from below with the cameras, while a side illumination by the laser is performed. The same mirror can also be used to illuminate the droplet from below, while the cameras are taking side view images of the droplet. The ratio of the images of the two cameras will be used subsequently to evaluate the temperature of the droplets.

2.3 Image processing and quantitative measurements

To obtain quantitative measurements of the temperature, a specific processing of the images is necessary. The steps of this processing, already described by Dunand *et al*. [6], include a correction for the possible non-linearity of the camera responses, a correction for geometric and chromatic aberrations of the imaging system, a repositioning of the pair of images given that the cameras may not have exactly the same field of view and a conversion of the fluorescence ratio into temperature by means of a calibration and a reference measurement. Corrections for the optical aberrations and the non-linearity of the detectors proved to be unnecessary with the present measurement system.

Pixel correspondence between the cameras

An offset of a few pixels between the images of the two cameras may remain despite a careful alignment of the beamsplitter. An accurate repositioning of the pair of images is thus needed before doing the ratio of both images to evaluate the temperature field. To do so, a calibration of the image coordinates is performed following a procedure already described by [9]. A 3rd order polynomial transform is created to obtain a perfect matching between the coordinates of the pixels in the images of the two cameras. This polynomial function is determined with the help of a regular grid of circular dots (diameter: 50 µm, spacing: 125 µm) positioned in front of the detection system. The grid pattern allows having at least 1500 control points in the image to determine the coefficient of the transform. This large number of control points insures an accurate positioning throughout the whole field of view. The residual error on the pixel positioning is estimated to be of the order of 10 µm in the worst case.

Temperature calibration

The fluorescence ratio R calculated by dividing the images of the two cameras is converted into temperature using a calibration curve. The calibration was carried out in a glass cell in which the fluorescent solution was heated progressively from 20°C to 80°C. Images were recorded in the two detection bands and the fluorescence ratio was determined. For a mixture $C_{SR640} = 0.7 \times 10^{-6}$ M and $C_{FL} = 2 \times 10^{-4}$ M (used later to investigate the drop impact), the temperature sensitivity of the fluorescence ratio R can be valuated at 2.7%/°C, meaning that $R/R_0 \approx \exp\{-0.027(T - T_0)\}$ in the case of water.

Reference measurement

A reference point is needed to convert the fluorescence ratio into temperature. Denoting f the calibration function and R the measured value of the fluorescence ratio, the temperature is given by:

$$T = f^{-1}\left(\frac{R}{R_0} f(T_0)\right) \quad (3)$$

where R_0 and T_0 are respectively the fluorescence ratio and the temperature at the reference point. R_0 is determined from images in which the droplet has just impinged the sapphire surface and T_0 is assimilated to the temperature measured by the thermocouple inserted in the thermal shield (Fig.2). It is assumed that the droplets do not heat up significantly when they travel in the hot air plume above the sapphire window.

3. Results and discussion

The experiments consist in varying the falling height of the droplet and thus its impact velocity V . Side and bottom views of the collision between the droplet and the wall are recorded for each impact condition. In a first step, water droplets are investigated. In a second step, ethanol droplets are considered to highlight the role played by the fluid properties (surface tension, boiling point,...). The Weber number $We = \rho V^2 d/\gamma$, which compares the kinetic energy of the droplet ($\sim \rho V^2$) to its surface energy ($\sim \gamma/d$), ranges from 10 to 140 for water droplets and from 30 to 140 for ethanol droplets. As ethanol has less surface tension than water, very low Weber numbers are not achievable with this experimental set-up. The magnification of the imaging system is adjusted for each experimental case in order to observe the whole droplet deformation, given that the maximum spreading diameter is increasing drastically with the Weber number.

3.1 Water droplets

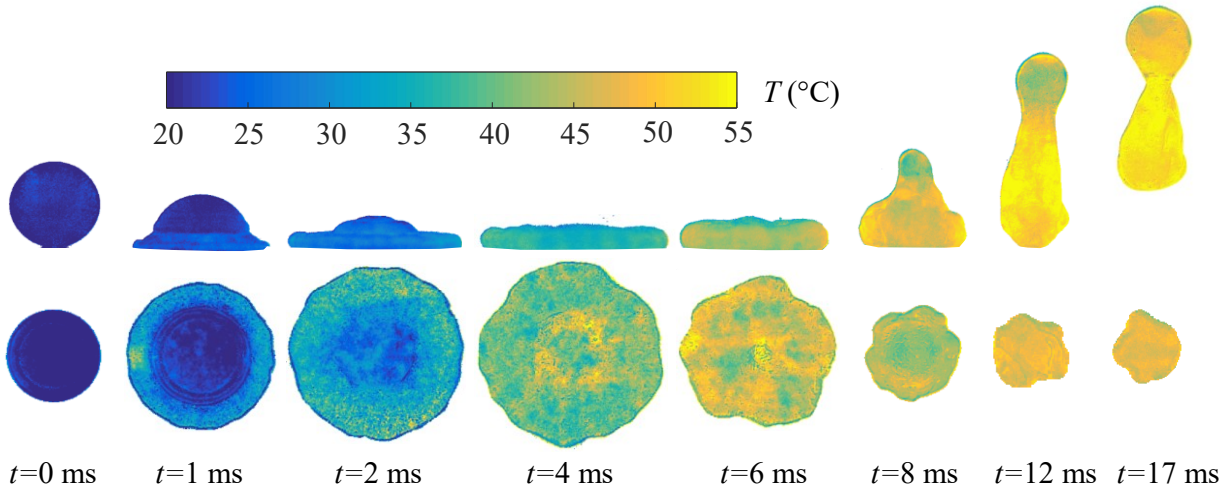

Fig. 4 Side and bottom views of the temperature field within an impacting water droplet at $We = 30.6$.

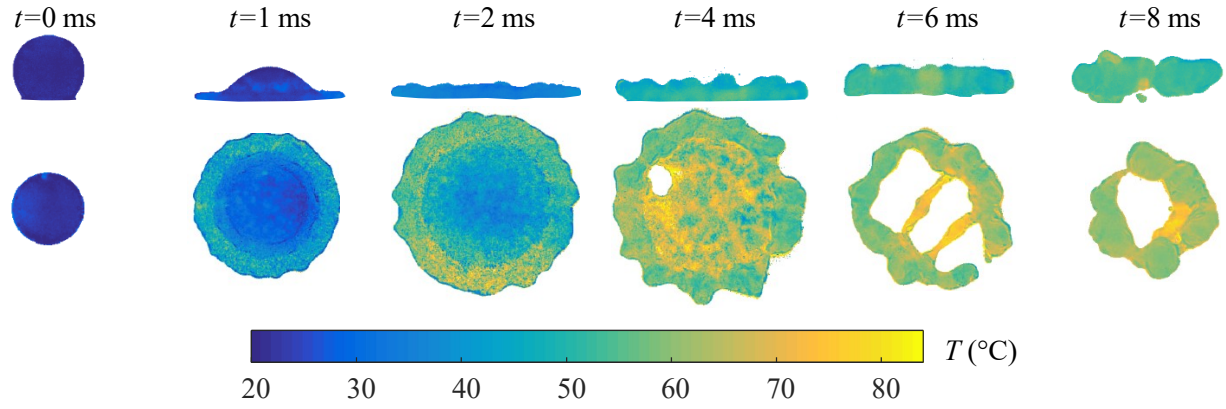

Fig. 5 Side and bottom views of the temperature field within an impacting water droplet at $We = 64.7$.

For water droplets, the wall temperature is set to 600°C, while the initial droplet temperature is maintained at 20°C. Figures 4 to 6 show instantaneous images of the temperature taken at different times during the impact. Side and bottom views are recorded for each impact condition. To interpret these images, it should be kept in mind that the imaging system does not provide optical sectioning of the droplet. The images roughly correspond to an average of the temperature in the depth of the droplet given that the depth of field of the cameras is several millimeters. Depending on the Weber number, different phases are observed: spreading and recoiling/bouncing or fragmentation/splashing.

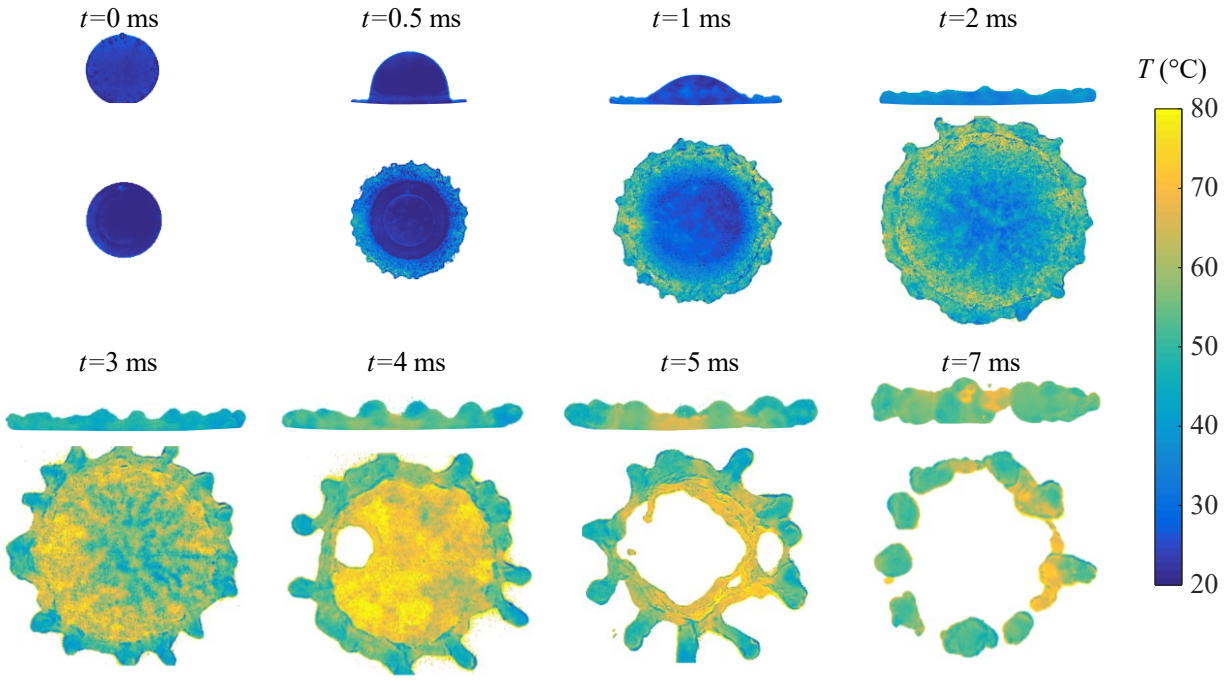

Fig. 6 Side and bottom views of the temperature field within an impacting water droplet at $We = 92$.

Spreading: The spreading phase lasts about 3-4 ms. For very low Weber number (typically ≤20), the heating is rather moderate during the spreading and it is diffcult to point out a region where the heating is more intense. Nevertheless, at higher Weber numbers (Figs.4-6), bottom views show a higher temperature band around the edge of the droplet at t = 1 ms and 2 ms. At these times, the ejected lamella is much thinner than the central region of the droplet, which helps observing a heating of the liquid in the bottom views. Provided a sufficiently large impact velocity, the lamella rapidly takes a gaussian shape surrounded by an annular rim, which is growing due to the liquid deceleration induced by the capillary forces opposed to the spreading [10]. Liquid is progressively heated while owing along the hot wall from the core of the lamella in the direction of the rim at the edge of the droplet. In Figure 6, the liquid temperature apparently reaches almost 80°C in the region of minimum thickness just before the entrance of the rim. Afterwards, in the rim, the hot liquid coming from the lamella rapidly mixes with colder liquid already accumulated there. Disturbances on the rim of the spreading drop can be easily observed for $We = 92$ at the early stage of the impact. These disturbances increase with time, leading to a spatter with characteristic fingers. Disturbances of smaller amplitudes also develop for lower Weber numbers but much more slowly. At t =4 ms and 5 ms, it can be seen for $We = 92$, both on the side and bottom view images, that the fingers are colder than the thinner regions in the rim.

Fragmentation of the rim and splashing: For $We = 92$, the previously mentioned fingers detach from the rest of the rim causing the fragmentation of the rim and ultimately the splashing of the droplet. The temperature of the secondary droplets resulting from the rim fragmentation evolves very little with time. It is of the order of 55°C-60°C for $We = 92$. In parallel, the lamella becomes so thin at the end of the spreading that it breaks. When this occurs, the temperature of the thin liquid sheet (about 80°C) is much larger than that of the surrounding liquid in the rim. Holes usually open in the vicinity of the rim where the lamella is thinner. The holes rapidly expand and hot liquid ligaments are created because of the opening and expansion of several holes at the same time.

Recoiling and bouncing: The recoiling of the droplet is initiated by the surface forces acting on the rim edge. The case $We = 64.7$ has some similarities with $We = 92$. Here also, several holes open the lamella at the end of the spreading phase. However, the rim does not break up and the empty space replacing the lamella narrows during the recoiling phase. For $We = 30.6$, the temperature is not uniform when the droplet takes ofrom the solid surface. The temperature is lower at the top end of the droplet where a satellite droplet nearly detaches. Hence, the flow induced by the droplet deformation inside of it is not capable of a full mixing of the liquid when the impact velocity is weak in the bouncing regime, typically for $We \leq 30$.

3.2 Ethanol droplets

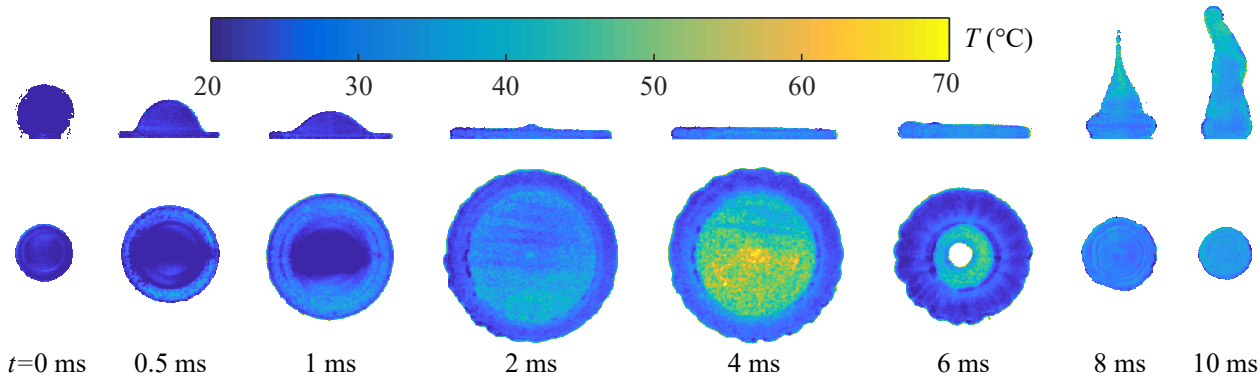

Fig. 7 Side and bottom views of the temperature field within an impacting ethanol droplet at $We = 92$.

For ethanol droplets, the wall temperature is set to 300°C, while the initial droplet temperature is maintained at 20°C. A new temperature calibration is achieved and a temperature sensitivity of the fluorescence ratio R is evaluated at 2.5 %/°C due to a small wavelength shift in dyes' emission spectra in ethanol.

Due to the lower boiling point and lower surface tension of ethanol, results obtained for impinging ethanol droplets show some differences with those of water droplets but also some similarities. Figure 7 show instantaneous images of the temperature taken at different times during the impact for a Weber number of 92, which best illustrates the experimental observations. Concerning the droplet deformation, during the spreading, the lamella also rapidly takes a gaussian shape surrounded by an annular rim. It can be noticed that disturbances of the rim are also observed for t = 2 ms and 4 ms and slightly increase with time. But these disturbances induced by Rayleigh-Taylor instabilities remain very moderate in comparison to the case of water for the same Weber number (fig. 6) and the ethanol droplet keeps almost a perfectly circular shape in the bottom views. As for water, bottom views show a higher temperature band around the edge of the droplet at t = 0.5 ms and 1 ms due the thinner ejected lamella than the central region of the droplet. Then, temperature becomes higher in the lamella. At the end of the spreading, roughly corresponding at time t = 4 ms, the temperature is higher at the center of the droplet. Almost at the same time, we can notice that a hole appears at the center of the droplet where the lamella becomes so thin that it breaks. This hole is visible on the bottom view in the recoiling phase at time t = 6 ms. But, unlike water, this hole does not expand leading to fragmentation but then totally disappears in the continuation of the receding. Another difference with water is that this hole is always situated at the center. As for water at moderate Weber numbers, the temperature is not uniform when the droplet takes off from the hot wall, but for ethanol droplet, the temperature is higher at the top end of the droplet. The temperature distribution is opposite to the one observed for $We = 30$ in the case of water, where no breakup of the drop is also observed. In both cases, a mixing takes place between the hot liquid coming from the previous lamella and the colder liquid coming from the rim, but the spatial orientation of the mixing is inversed.

3.3 Final heating of the droplets: effect of the impact velocity

Figure 8 shows the final heating of the droplet for all the tested impact velocities. The reported values are calculated from the mean temperature of the side and bottom view images, presented for some Weber numbers in Figs.4-7. The final heating is plotted for water and ethanol droplets. Concerning the water droplets, in a first phase, the heating increases with increasing Weber number, until a plateau is reached. This plateau corresponds to the apparition of the splashing

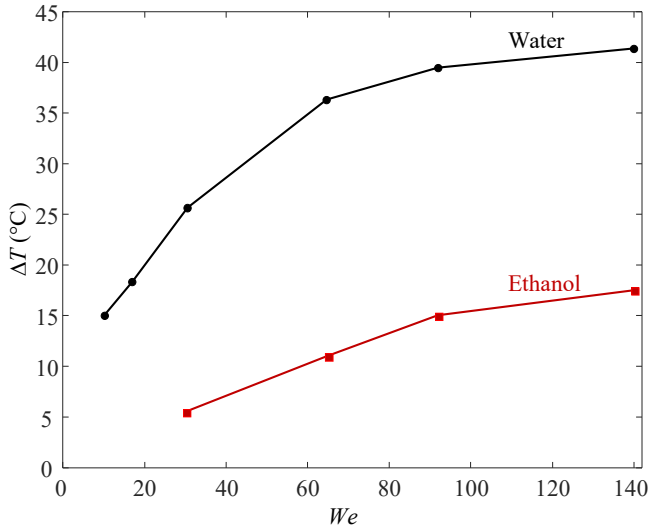

Fig. 8 Evolution of the spatially averaged final droplet heating with the Weber number for water and ethanol droplets.

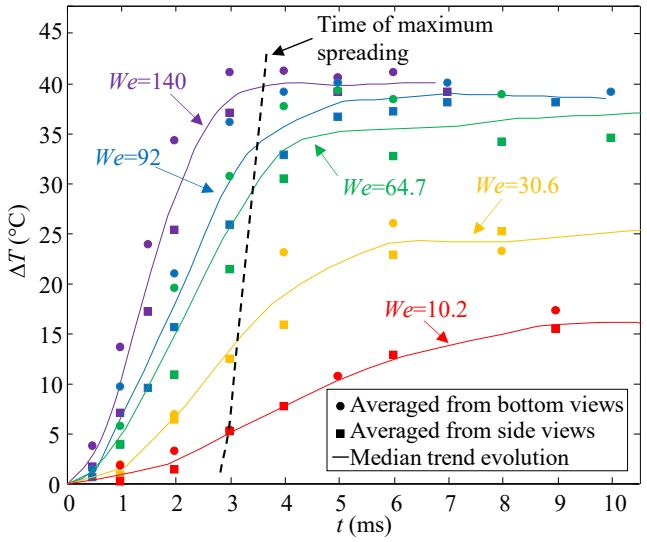

Fig. 9 Temporal evolution of the spatially averaged droplet heating in the case of water for different Weber numbers.

regime in the case of water. At low impact velocity, the heating period covers both the spreading and the recoiling phases as seen in Fig. 4. On the contrary, most of the heating takes place during the spreading for $We \geq 64.7$ (Figs. 5-6). For higher Weber numbers, most of the heating has reached (or is about to reach) its final value just before that the fragmentation of the rim takes place (Fig. 9). Hence, measurements reveal that the fragmentation of the droplet in itself has little effect on the final heating [7]. As the Weber number increases, the spreading surface increases which improves the heat exchange during the spreading phase. Nonetheless, the liquid is accumulated faster in the rim where the heat transfer rate with the wall seems to be poor. For the ethanol droplets, the trend is similar but two major differences can be noticed. As the fragmentation of the rim is not observed even for Weber number of 140, a plateau seems to be reached for higher We. As for water, the liquid trapped in the rim does not heat significantly. In the center of the lamella, the heating becomes also limited when the liquid temperature becomes very close to the boiling point (78°C for ethanol). Another comment is that the final heating of the ethanol droplets is lower than for water ones. This point can be due to the lower boiling point of ethanol. The vapor layer under the drop is certainly thicker than for water droplets therefore ethanol droplets are more insulated from the hot solid surface and the final heating of the droplet is less important. It should be interesting to estimate the heat extracted from the wall to manage a heat balance and evaluate in which proportion the cooling of the solid wall is due to the sensible heating of the liquid for ethanol droplets. In the case of the millimeter-sized water

droplets, complementary measurements based on IR thermography have shown that almost all the cooling of the solid wall results from the sensible heating of the liquid [11].

4. Conclusion

The heating of the impacting droplet onto a solid surface in the film boiling regime was quantified accurately using a non-intrusive optical technique: the two-color planar LIF. This study demonstrates the capabilities of the two-color laser-induced fluorescence thermography to perform an accurate instantaneous temperature imaging of dispersed liquid flows. The couple of dyes fluorescein disodium/sulforhodamine 640 should be recommended at high laser irradiances in the saturated regime of excitation of the fluorescence. Measurements show an important effect of the Weber number on the heat transfers. As the Weber number increases, the exchange surface increases which induces an increase in the heating of the liquid. However, when increasing the Weber number, the influence of the impact velocity becomes less and less noticeable. There is almost a saturation of the heat extracted from the solid surface in the splashing regime of impact. This trend was observed for water droplets. For ethanol droplets, the fragmentation of the rim is not observed even for Weber number of 140, a plateau seems to be reached for higher We than for water. The final heating of the ethanol droplets was found to be lower than for the water droplets. This is probably due to the thicker vapor layer under the ethanol droplets during the impact process.

5. Acknowledgements

The authors acknowledge the financial support of the Lorraine region through the CPER ENERBATIN project.

References

[1] Liang G, Mudawar I (2017) Review of drop impact on heated walls. Int J Heat and Mass Transfer 106:103-126.

[2] Jung J, Jeong S, Kim,H (2016) Investigation of single-droplet/wall collision heat transfer characteristics using infrared thermometry. Int J Heat and Mass Transfer 92:774-783.

[3] Dunand P, Castanet G, Gradeck M, Maillet D, Lemoine F (2013) Energy balance of droplets impinging onto a wall heated above the leidenfrost temperature. Int J Heat and Fluid Flow 44:170-180.

[4] Lemoine F, Castanet G (2013) Temperature and chemical composition of droplets by optical measurement techniques: a state-of-the-art review. Exp in Fluids 54(7).

[5] Castanet G, Lienart T, Lemoine F (2009) Dynamics and temperature of droplets impacting onto a heated wall. Int J Heat and Mass Transfer 52(3-4):670-679.

[6] Dunand P, Castanet G, Lemoine F (2012) A two-color planar lif technique to map the temperature of droplets impinging onto a heated wall. Exp in Fluids 52(4):843-856.

[7] Chaze W, Caballina O, Castanet G, Lemoine F (2016) The saturation of the fluorescence and its consequences for laser-induced fluorescence thermometry in liquid flows Exp in Fluids 57(4): 58.

[8] Sutton JA, Fisher BT, Fleming JW (2008) A laser-induced fluorescence measurement for aqueous fluid flows with improved temperature sensitivity. Exp in Fluids 45(5):869-881.

[9] Sakakibara J, Adrian R (1999) Whole field measurement of temperature in water using two-color laser induced fluorescence. Exp in Fluids 26(1-2):7-15.

[10] Castanet G, Caballina O, Lemoine F (2015) Drop spreading at the impact in the leidenfrost boiling. Phys Fluids 27(6):063302.

[11] Chaze W, Castanet G, Caballina O, Maillet D, Pierson JF, Lemoine F (2017) Instantaneous heat transfers at the impact of a droplet onto a hot surfaces in the film boiling regime. In 28th Conference on Liquid Atomization and Spray Systems.